Enhanced vibrational-mode-selective two-step excitation using ultrabroadband frequency-entangled photons

Hisaki Oka

Phys. Rev. A **97**, 063859 — Published 29 June 2018

DOI: 10.1103/PhysRevA.97.063859

Enhanced vibrational-mode-selective two-step excitation using ultrabroadband frequency-entangled photons

Hisaki Oka[1,*]

[1]*Niigata University, 8050, Ikarashi 2-no-cho, Nishi-ku, Niigata 950-2102, Japan*

(Dated: May 25, 2018)

Abstract

We theoretically investigate strongly-enhanced vibrational-mode-selective two-step excitation by ultrabroadband frequency-entangled photons. A diatomic molecule having three sets of vibronic states is used to evaluate the excitation efficiency of the two-step excitation. We show that the photon entanglement has little influence on the populations of intermediate vibrational modes of intermediate states but selectively increases the population of a single vibrational mode of excited states, resonant with the total energy of the entangled photons. For an ultrashort pulse close to a monocycle with high degree of entanglement, the population of the vibrational mode is enhanced 2500 times as large as that by uncorrelated photons and the selectivity nearly reaches unity. Our results indicate that the two-step excitation with ultrabroadband frequency-entangled photons can achieve highly-selective and strongly-enhanced excitation of a single vibrational mode.

PACS numbers: 42.50.-p, 42.65.Sf

*Email address: h-oka@eng.niigata-u.ac.jp

I. INTRODUCTION

Two photon process has a wide application to various leading-edge techniques, such as two-photon microscopy [1], three-dimensional optical storage memory [2], and coherent control of molecular processes [3]. Generally, two-photon process is divided into two types, namely, two-step excitation (TSE), in which each of two photons is absorbed sequentially by intermediate and excited states, and two-photon absorption (TPA), in which two photons are simultaneously absorbed by excited states via virtual excitation of intermediate states. In particular, TPA driven by entangled photons has been extensively investigated in recent years since the non-classical linear intensity dependence of excitation was theoretically predicted [4, 5] and experimentally demonstrated [6] in the 1990s. Applications of entangled photons to TPA are now extending to various next-generation technologies such as quantum optical spectroscopy [7–13], quantum coherent tomography [14, 15], molecular coherent control by non-classical light [16, 17], and quantum plasmonics [18]. Though an efficient TPA requires the simultaneous absorption of two photons, the entangled photons automatically satisfy this condition because they have an inherent coincidence based on the quantum correlation which does not exist in the classical light. Consequently, though seemingly contradictory, TPA by low-intensity light with high two-photon flux density can be realized with entangled photons.

In order to maximally exploit the TPA with entangled photons, ultrabroadband frequency-entangled photons are desired. Fortunately, by using the chirped quasi-phase-matching technique [19], we can experimentally obtain entangled photons with a frequency range of $\sim$ 160 THz [20]. However, at the same time, the wider bandwidth of entangled photons raises an emerging problem such that intermediate states are really excited as a consequence of the broad frequency band and hence TSE via the real excitation of intermediate states occurs. For the applications based on TPA, such as quantum coherent tomography and virtual state spectroscopy, this situation might be unfavorable because the real excitation of intermediate states might decrease the quantum efficiency of the target molecular process induced in the excited states.

Generally, the population obtained from TSE is often much larger than that obtained from TPA. Therefore, TSE is preferable for the molecular processes such as photoionization and photodissociation, because they require only high excitation of high-energy levels. However,

conventional studies of the two-photon excitation using entangled photons focus almost only on TPA and few studies on TSE by entangled photons have been reported. This is because the inherent coincidence of the entangled photons is perfectly suited to TPA and the coincidence of photons is seemingly unsuitable for TSE because in TSE each of the two photons is sequentially absorbed. However, in our previous work [21], we have shown that the entangled photons can enhance the efficiency of not only the TPA but also the TSE. Although the analysis is restricted to a simple three-level system, the population of an excited state is enhanced a thousand times as large as that by uncorrelated photons. If the molecular process via the real excitation of molecular vibrational states can be strongly enhanced by using entangled photons, the application range of the entangled photons will be much broader.

In this study, we analyze in detail the TSE for a molecular system by using ultrabroadband frequency-entangled photons in terms of how photon entanglement can enhance the population of molecular vibronic states. By taking a diatomic molecule Na_2 as an example, we show that photon entanglement has little influence on the populations of intermediate vibrational modes but highly selectively increases the population of a single vibrational mode of excited states, which is resonant with the total energy of the entangled photons. For an ultrashort pulse close to a monocycle with high degree of entanglement, the population of the vibrational mode is enhanced 2500 times as large as that by uncorrelated photons and the selectivity nearly reaches unity. These results indicate that the highly-efficient vibrational-mode-selective excitation can be realized by the TSE with ultrabroadband frequency-entangled photons.

The rest of this paper is organized as follows. In Sec. II, a theoretical model of the one-dimensional input-output photon field interacting with Morse oscillators is introduced and the formulation of the entangled photons is given. In Sec. III, we analyze in detail the quantum dynamics of TSE driven by the entangled photons and the dependence of TSE efficiency on the spectral width of the entangled photons. In Sec. IV, we summarize and discuss our results.

II. MODEL

A. One-dimensional input-output photon field interacting Morse oscillators

As a theoretical model, we consider a one-dimensional input-output photon field interacting with a molecular system, as depicted in Fig. 1. The incident entangled photons propagate along the r-axis from $r < 0$ and interact with the molecular system positioned at $r = 0$. The molecular system consists of three sets of vibronic states with vibrational modes v: the ground state $|g\rangle$, the intermediate states $\{|m_v\rangle\}_v$, and the excited states $\{|e_{v'}\rangle\}_{v'}$, where for the ground state we consider only the lowest vibrational mode $v = 0$, assuming a supersonic molecular beam, and omit v. The eigenenergies of these vibronic states are denoted by ω_g, ω_{m_v}, and $\omega_{e_{v'}}$. We consider only the transitions between $|g\rangle$ and $\{|m_v\rangle\}_v$ and between $\{|m_v\rangle\}$ and $\{|e_{v'}\rangle\}_{v'}$, as denoted by the arrows in Fig. 1, and the direct transition from $|g\rangle$ to $\{|e_{v'}\rangle\}_{v'}$ by one photon and the vibrational relaxations within $\{|m_v\rangle\}_v$ and $\{|e_{v'}\rangle\}_{v'}$ are ignored on the assumption of a ultracold molecule, for simplicity.

For the molecular system, we adopt a diatomic molecule and approximate the adiabatic potential curve by the Morse potential because we can analytically obtain the vibrational eigenfunctions [22]. The Morse potential for the vibronic states of ℓ is defined as

$$V_\ell(x) = D_\ell(\{1 - \exp[-(x - x_0^\ell)/a_\ell]\}^2 - 1), \tag{1}$$

where ℓ implies g, m, or e. x is the displacement of internuclear separation from the equilibrium position of x_0. D and a are the depth and range of the potential, respectively. The eigenenergies in the potential, ω_g, ω_{m_v}, and $\omega_{e_{v'}}$, are given by

$$\omega_{\ell_v} = \epsilon_\ell + \omega_\ell(v + 1/2) - \omega_\ell\chi(v + 1/2)^2 \tag{2}$$

with $\omega_\ell = (2D_\ell/a_\ell^2\mu)^{1/2}$ and $\chi = (8a_\ell^2 D_\ell\mu)^{-1/2}$, where ϵ denotes the minimum of the potential energy, χ characterizes the anharmonicity of the Morse potential, and μ is the reduced mass of two nuclei. The corresponding vibrational eigenfunctions are given by $\xi_v(y) = N_{j,v}\exp(-y/2)y^{j/2-v}L_v^{j-2v}(y)$ with $y = (j + 1)\exp[-(x - x_0)/a]$ and $j = 2a(2\mu D)^{1/2} - 1$, where the index of ℓ is omitted to avoid a complicated description. L represents the generalized Laguerre polynomials and N is the normalized coefficient given by $N_{j,v} = [v!(j - 2v)/a\Gamma(j - v + 1)]^{1/2}$, where Γ is the gamma function.

In the actual calculations, a Na_2 molecule is used by reference to Refs. [23, 24] because the multiphoton ionization has been analyzed in detail and the Morse parameters are already given. In this study, the Morse parameters used are as follows: $\epsilon_g = 0$, $D_g = 0.7466$ eV, $a_g = 2.2951 a_B$, and $x_0^g = 5.82 a_B$ for $|g\rangle$ $(1^1\Sigma_g^+)$; $\epsilon_m = 1.8201$ eV, D_m= 1.0303 eV, $a_m = 3.6591 a_B$, and $x_0^m = 6.87 a_B$ for $|m\rangle$ $(1^1\Sigma_u^+)$; $\epsilon_e = 3.7918$ eV, D_e= 0.5718 eV, $a_e = 3.1226 a_B$, and $x_0^e = 7.08 a_B$ for $|e\rangle$ $(2^1\Pi_g)$; where a_B is the Bohr radius. $\mu = 19800$ is used in the units of electron mass. The calculation results of ω_g, ω_{m_v}, and $\omega_{e_{v'}}$ for the Na_2 molecule are shown in Fig. 1, where ω_{m_v} and $\omega_{m_{v'}}$ are described up to $v = 140$ and $v' = 89$, respectively.

For the optical transition, we adopt the Franck-Condon approximation. When the time scale of the light-molecule interaction is shorter than that of molecular vibration, the optical transition rate between the two vibronic states can be approximated by the product of the electric-dipole transition rate and the Franck-Condon factor. The Franck-Condon factor is given by

$$F_{v,\nu} = \left| \int dx \; \xi_\nu^l(x) \xi_v^\ell(x) \right|^2 . \tag{3}$$

$F_{0,v} \equiv F_v$ for the transition between $|g\rangle$ and $\{|m_v\rangle\}_v$ and $F_{v,v'}$ for the transition between $\{|m_v\rangle\}_v$ and $\{|e_{v'}\rangle\}_{v'}$ are shown in Figs. 2(a) and (b), respectively. For the intermediate states $\{|m_v\rangle\}_v$, the vibrational states from $v = 0$ to $v = 140$ are bound states. However, the bound states up to $v = 20$ mainly contribute to photon absorption from $|g\rangle$. For the excited states, the vibrational states from $v = 0$ to $v = 89$ are bound states. Similarly to the intermediate states, the transition between $\{|m_v\rangle\}$ and $\{|e_{v'}\rangle\}$ mainly occurs in a specific range of $v \approx v'$. Thus, though many vibrational modes exist, only a part of the total modes contributes to the actual optical transitions.

B. Hamiltonian and quantum dynamics

In the calculation of quantum dynamics, we omit the degrees of freedom of polarization of light by assuming linearly-polarized light for simplicity. Setting natural units of $\hbar = c = 1$ and using the dispersion relation of $\omega = ck = k$, the Hamiltonian of the whole system can

be expressed as

$$\begin{aligned}\hat{H} &= \int dk\ k\hat{a}^\dagger(k)\hat{a}(k) + \sum_{v'}\omega_{e_{v'}}|e_{v'}\rangle\langle e_{v'}| + \sum_{v}\omega_{m_v}|m_v\rangle\langle m_v| \\ &+ \sum_{v}\int dk(\gamma_{m_v}F_v/\pi)^{1/2}\left[|m_v\rangle\langle g|\hat{a}(k) + \hat{a}^\dagger(k)|g\rangle\langle m_v|\right] \\ &+ \sum_{v,v'}\int dk(\gamma_{e_{v,v'}}F_{v,v'}/\pi)^{1/2}\left[|e_{v'}\rangle\langle m_v|\hat{a}(k) + \hat{a}^\dagger(k)|m_v\rangle\langle e_{v'}|\right], \end{aligned} \tag{4}$$

where $\hat{a}(k)$ $\left[\hat{a}^\dagger(k)\right]$ is the annihilation (creation) operator of a photon with energy k. γ_{m_v} is the relaxation rate between $|g\rangle$ and $|m_v\rangle$ and $\gamma_{e_{v,v'}}$ is the relaxation rate between $|m_v\rangle$ and $|e_{v,v'}\rangle$. In this study, we set $\gamma = \gamma_{m_v} = \gamma_{e_{v,v'}} = 6$ MHz, for simplicity, and the Franck-Condon factor can be simply introduced by multiplying γ.

The dynamics of the whole system can be calculated from the Schrödinger equation,

$$\frac{d}{dt}|\Psi(t)\rangle = -i\hat{H}|\Psi(t)\rangle \tag{5}$$

with a superposition state of $|\Psi\rangle$, given by

$$\begin{aligned}|\Psi\rangle = 2^{-1/2}\int dk\int dk'\psi_{2p}(k,k')\hat{a}^\dagger(k)\hat{a}^\dagger(k')|0\rangle|g\rangle + \sum_v\int dk\psi^m_{1p}(k,v)\hat{a}^\dagger(k)|0\rangle|m_v\rangle \\ + \sum_{v'}\psi^e_0(v')|0\rangle|e_{v'}\rangle,\end{aligned} \tag{6}$$

where $\psi_{2p}(k,k')$ is the two-photon joint amplitude of the incident pulse at $|g\rangle$, ψ^m_{1p} is the one-photon state at $|m\rangle$, and ψ^e_0 is the zero-photon state at $|e\rangle$. The argument t of ψ is omitted for simplicity. The initial state of the whole system $|\Psi(0)\rangle$ is given by the first term in Eq. (6), i.e., $\psi^m_{1p}(k) = \psi^e_0 = 0$, and the whole wave function is normalized to be $\langle\Psi|\Psi\rangle = 1$. From Eqs. (4), (5), and (6), the Schrödinger equations for ψ can read

$$\frac{d}{dt}\psi_{2p}(k,k') = -i\left(k+k'\right)\psi_{2p}(k,k') - i\sum_v 2^{-1/2}\gamma_v\left\{\psi^m_{1p}(k,v) + \psi^m_{1p}(k',v)\right\}, \tag{7}$$

$$\frac{d}{dt}\psi^m_{1p}(k,v) = -i\left(k+\omega_{m_v}\right)\psi^m_{1p}(k,v) - i2^{1/2}\gamma_v\int dk'\psi_{2p}(k,k') - i\sum_{v'}\gamma_{v,v'}\psi^e_0(v'), \tag{8}$$

$$\frac{d}{dt}\psi^e_0(v') = -i\omega_{e_{v'}}\psi^e_0(v') - i\sum_v\gamma_{v,v'}\int dk\psi^m_{1p}(k,v), \tag{9}$$

where $\gamma_v = (\gamma_{m_v}F_v/\pi)^{1/2}$ and $\gamma_{v,v'} = (\gamma_e F_{v,v'}/\pi)^{1/2}$. The populations of vibronic states are calculated e.g. by $\langle e'_v\rangle = |\langle 0|\langle e'_v|\Psi(t)\rangle|^2 = |\psi^e_0|^2$.

C. Frequency-entangled photons with energy-anticorrelation

In order to describe the two-photon joint amplitude $\psi_{2p}(k,k')$, we first define a spatiotemporal one-photon wavepacket $\varphi(r)$, choosing a Gaussian form for simplicity. Similarly in Sec. II B, we use natural units of $\hbar = c = 1$. According to Ref. [16], $\varphi(r)$ is given by

$$\varphi(r) \propto \exp\{-(r-r_0)^2/\sigma_r^2 + ik_0(r-r_0)\}, \tag{10}$$

where r_0 is the spatial center position of wavepacket at $t = 0$, σ_r is the coherent length of the wavepacket, and k_0 is the central energy of the photon pulse. The one-photon wavepacket in the k representation, $\varphi(k)$, can be obtained by Fourier transforming $\varphi(r)$ to the frequency domain, given by

$$\varphi(k)e^{-ikr_0} = \frac{1}{\sqrt{2\pi}}\int_{-\infty}^{\infty} dr\varphi(r)\exp(-ikr) \tag{11}$$

with $\varphi(k) \propto \exp\{-(k-k_0)^2/4\sigma^2\}$ where $\sigma = \sigma_r^{-1}$ is the spectral width of the wavepacket.

Using the one-photon wavepacket, we can now describe the two-photon joint amplitude $\psi_{2p}(k,k')$. For comparison, we consider two photon pairs, namely, uncorrelated photon pair and entangled photon pair with energy anticorrelation. Since uncorrelated photon pair has no correlation between the two photons, the two-photon joint amplitude can be described simply by the product of one-photon wavepackets, given by

$$\psi_{2\mathrm{p}}(k,k') = \varphi(k)\varphi(k')e^{-ikr_0}e^{-ik'r_0}. \tag{12}$$

On the other hand, for the entangled photon pair with energy anticorrelation, $\psi_{2p}(k,k')$ can be described as

$$\psi_{2\mathrm{p}}(k,k') = \varphi(k)\delta(k+k'-2k_0)e^{-ikr_0}e^{-ik'r_0}. \tag{13}$$

$\delta(k+k'-2k_0)$ ensures the quantum-mechanical energy anticorrelation of the two photons: one photon with an energy $k = k_0 - \Delta$ is accompanied by the other photon with an energy $k' = k_0 + \Delta$, conserving the total energy of $2k_0$. By Fourier transforming to the time domain, this property implies that the photon pair inherently has a time coincidence. Experimentally, this photon state can be obtained, e.g. from the spontaneous parametric down-conversion.

Generally, the energy anticorrelation of experimentally-created entangled photons, e.g. from the spontaneous parametric down-conversion, is not the Dirac δ function as in Eq. (13) but has a linewidth due to spontaneous emission. In this study, we replace the δ function

by a Gaussian form, defined as $\phi(k) = (\sigma_s^2\pi)^{-1/4}\exp(-k^2/4\sigma_s^2)$, so that $\phi(k)$ corresponds to the δ function in the limit of $\sigma_s \to 0$. For the parametric down-conversion, σ_s is determined by the pulse width of pump light. Though $\sigma_s \approx 100$ kHz can be experimentally achieved by using a narrow-spectrum cw laser, we use σ_s =500 GHz or 100 GHz in the following calculation to reduce the computational task.

III. RESULTS

In this section, we analyze the TSE by frequency-entangled photons in terms of how photon entanglement can enhance the population of molecular vibronic states and how the excitation efficiency depends on the spectral width σ. In the following calculation, we numerically solve the Eqs. (7), (8), and (9) by discretizing the photon fields. Concretely, continuous photon fields are discretized by converting from $(\delta k)^{-1}\int dk$ and $(\delta k)^{1/2}\hat{a}(k)$ to $\sum_k$ and $\hat{a}_k$, respectively, where $\delta k = 2\pi/R$ is the mode spacing and R is the length of calculation region. We use $\delta k = 100$ GHz to reduce computational task and the total number of photon modes is then 49014001 (7001 modes per photon), which corresponds to 3.5 times of the full width of $2\sigma = 200$ THz. The central energy of entangled photons is set to $2k_0 = \omega_{v'=18}$ (≈ 4.0024 eV). For vibrational modes, all the bound states are considered. The discretized Schrödinger equations are solved by using the 4th-order Runge-Kutta method.

We first calculate the dynamics of intermediate states in TSE. For comparison, the populations for uncorrelated and entangled photons are shown in Fig. 3, where the vibrational modes up to $v = 15$ are plotted. The parameters for Na_2 are the same as those in Fig. 2 and for incident photons $\sigma = 10$ THz and $\sigma_s = 500$ GHz are used. The horizontal axis $r\sigma$ is the spatial center position of the incident photons normalized by the pulse width $\sigma_r = \sigma^{-1}$. When the incident photons reach $r = 0$, the molecular system absorbs one photon and the intermediate states are excited. For both uncorrelated and entangled photons, $\langle m_v \rangle$ does not decrease to zero after the incident photons have passed by the molecule and remains almost constant. This is a well-known TSE process where the intermediate states are really excited. However, there is a little difference between the uncorrelated and entangled photons in absorbing photon; the photon in the entangled photons is slowly and resonantly absorbed by the molecule, whereas for uncorrelated photons the oscillation of population, commonly found in near-resonant absorption, appears. Interestingly, though there is thus

a little difference in absorbing photon, the resultant populations of $\langle m_v \rangle$ are almost the same for uncorrelated and entangled photons. This implies that the quantum entanglement between two photons have little influence on the population in the one-photon absorption from $|g\rangle$ to $\{|m_v\rangle\}_v$.

Figure 4 shows the population dynamics of excited states $\langle e_{v'} \rangle$ in the TSE. The calculation parameters are the same as those in Fig. 3. For the uncorrelated photons (Fig. 4a), many vibrational modes are simultaneously excited owing to short pulse excitation with a spectrally broad bandwidth. The maximum population is achieved for $v' = 12$ in spite of the resonant excitation of the vibrational mode of $v' = 18$. This is because that the Franck-Condon factors $F_{v,v'=18}$ are very small for $v < 12$ and $F_{v=10,v'=12}$ becomes large as can be seen in Fig. 2. For the entangled photons (Fig. 4b), however, the resonant excitation of the vibrational mode of $v' = 18$ is highly selectively excited and strongly enhanced. For the present parameters, $\langle e_{v'=18} \rangle$ is enhanced approximately 60 times as large as that by uncorrelated photons. If we define a mode selectivity as $S = \langle e_{v'=18} \rangle / \sum_{v'} \langle e_{v'} \rangle$, S reaches up to $S \approx 0.9999$ for entangled photons, whereas $S = 0.0396$ for uncorrelated photons. In general, selective excitation of molecular vibronic states requires detailed Franck-Condon analysis and pulse shaping techniques. Using entangled photons, however, high selectivity and enhancement of excitation efficiency can thus be easily and concurrently achieved.

According to the previous studies for an atomic system [25, 26], the enhancement by entangled photons can be further increased by both broadening the spectral width σ and by narrowing σ_s, corresponding to strengthening the quantum correlation between the two photons. Figure 5 shows the dependence of the enhancement ζ on σ for the range from 5 to 100 THz, where ζ is defined by the ratio of the population obtained from entangled photons to that obtained from uncorrelated photons. The parameters are the same as those in Figs. 3 and 4 except for $\sigma_s = 100$ GHz. The symbol $\square$ denotes ζ for the vibrational mode of $v' = 18$. Similarly to the result for a simple three-level system in Ref. [21], large enhancement can be achieved; ζ exhibits a linear dependence with σ and reaches 2500 at $\sigma = 100$ THz for the present parameters. The symbol $\circ$ denotes ζ for the total population of the vibrational modes in the excited states. In contrast to the case of $v' = 18$, ζ slightly decreases in the range from 5 to 20 THz, and then linearly increases from 20 THz. The value of ζ for the total population is considerably smaller than that for $v' = 18$: for the present parameters $\zeta = 30$ at $\sigma = 100$ THz. Though not shown, the selectivity S for entangled photons exceeds

0.9995 for all the range from 5 to 100 THz. Thus highly-efficient vibrational-mode-selective TSE can be realized with ultrabroadband frequency-entangled photons.

We refer to why the σ-dependence of ζ for the total population suddenly changes at $\sigma = 20$ THz. This is because that the vibrational number of v yielding the maximum $\langle m_v \rangle$ changes with the increase in σ. Since the total energy of entangled photons is $2k_0 \approx 4.0024$ eV, the central energy of one photon is $k_0 \approx 2.0012$ eV, which is nearly resonant to $\omega_{v=13}$. As can be seen in Fig. 2(a), the value of $F_{v=13}$ is not so large and hence the maximum population of intermediate states is obtained at smaller v yielding larger F_v for $\sigma < 20$ THz. For example, for $\sigma = 10$ THz, the maximum $\langle m_v \rangle$ is obtained at $v = 10$ as shown in Fig. 3. For $\sigma \geq 20$ THz, however, the spectral width of photons covers the peak of F_v and hence $\langle m_v \rangle$ always becomes maximum at $v = 7$. Consequently, ζ of the total population monotonically increases for $\sigma \geq 20$ THz. Thus, σ-dependence of ζ slightly changes near the peak value of the Franck-Condon factor.

Finally, we analyze how ζ depends on σ_s. Taking a parametric down-conversion as an example, σ_s can be changed by varying spectral width of pump light. In this study, however, we connect σ_s to the degree of entanglement, for generalization. The degree of entanglement can be evaluated by using the entropy of entanglement, namely, relative entropy of entanglement [27] or entanglement of formation [28]. Generally, relative entropy of entanglement is used for mixed states not considered in this study, and therefore we adopt the entanglement of formation. The entanglement of formation, E, is defined as

$$E = -\mathrm{Tr}[\rho' \log_d \rho'] \text{ with } \rho' = \mathrm{Tr}'[\rho] \tag{14}$$

where $\rho = |\psi\rangle\langle\psi|_{\text{photons}}$ is the density operator of input entangled photons, ρ' indicates the density operator partially-traced for one photon, and d is the dimension of ρ. Figure 6(a) shows the dependence of E on σ_s for σ =50 THz. E exhibits drastic increase for smaller σ_s, and at $\sigma_s = 100$ GHz, corresponding to Fig. 5, $E \approx$0.83 is achieved. The dependences of ζ for $v' = 18$ and S on E are shown in Fig. 6(b), where the data only for $E = 0$ is obtained from uncorrelated photons and vibrational modes of intermediate and excited states are cut off at $v = 30$ and $v' = 30$ to shorten computation time. Both ζ and S increase very gradually for $E \lesssim 0.5$, in which ζ is at most 10 and S is below 0.1. On the other hand, for $E \gtrsim 0.5$, both E and S drastically increase, and in particular ζ exceeds 1000 at $E \approx 0.83$ and S becomes nearly unity for $E \gtrsim 0.77$. Thus, strong enhancement and high selectivity

are achieved for high E, and conversely this indicates that we cannot achieve large ζ and high S at low E even for ultra broadband entangled photons.

IV. SUMMARY AND DISCUSSION

In summary, we have analyzed the enhanced vibrational-mode-selective TSE using the ultrabroadband frequency-entangled photons. By taking a cold diatomic molecule Na_2 as an example, we have shown that photon entanglement has little influence on the populations of vibrational modes of intermediate states but highly selectively increases the population of a single vibrational mode of excited states, which is resonant with the total energy of the entangled photons. The TSE excitation efficiency can be enhanced 2500 times by the ultrabroadband frequency-entangled photons with spectral width of $2\sigma = 200$ THz, whereas the enhancement of the total population of excited states is at most 30 times. The selectivity S of vibrational mode selection by the entangled photons nearly reaches unity for all the range from $\sigma = 5$ to 100 THz. The strong enhancement and high selectivity occur when high E is achieved. These results thus indicate that highly-efficient vibrational-mode-selective excitation can be realized by using the ultrabroadband frequency-entangled photons with high E.

From the results of this study, the enhancement of TSE by entangled photons is caused by the energy anticorrelation in the frequency domain rather than the coincidence of two photons in the time domain required in TPA. This fact is quite powerful for the application to measurement methods, such as pump-probe method, Raman process, and frequency-comb technique, because we can introduce and control the degree of freedom of time delay (or phase) between the two photons constituting entangled photons. Combining these conventional methods and vibrational-mode-selective excitation by ultrabroadband frequency-entangled photons, new approaches for measuring molecular structure and wavefunction might be promising.

Throughout this study, we have ignored the effects of vibrational relaxation on the TSE process on the assumption of a cold molecule. If we consider the application of entangled photons to molecular processes in real situations, we must consider the effects of vibrational relaxation (phase and thermal relaxations). A straightforward way of including the relaxation effects is to calculate the dynamics using quantum master equation. However, to

accurately calculate the broadband frequency-entangled photons, an enormous number of photon modes are required. Even in this study, we have used 49014001 modes for the entangled photons, and hence the extension to the quantum master equation will be hard from the viewpoint of computational task. The analysis using stochastic Schrödinger equation might be useful because we can directly extend the method presented in this study.

Finally, we refer to the effects of emission rate γ. For low-intensity excitation, the population is primarily determined by γ of the target energy level because induced absorption of photons is negligibly small. Therefore, if we want to further increase the value of the population of vibrational modes, we have to choose or design a molecule with large γ. Although we can now utilize a high-intensity source of entangled photons, highly intense light might lead to the deterioration and structural change of target molecular processes, and therefore we have to choose a specific material with γ. One possible way of avoiding this restriction is to utilize the nanoantenna effect as suggested in Ref. [18] and the cavity QED effects for molecules as in Ref. [29, 30]. The former technique is summarized as indirect enhancement of the absorption cross-section of molecules using the antenna effect of nanoparticles and the latter is summarized as direct enhancement of γ of molecules through cavity QED effects. These techniques can be directly and simply applied to the TSE by entangled photons. We hope that our results in this study facilitate the applications of entangled photons to various fields.

Acknowledgments

This work was supported by JSPS KAKENHI Grant No. JP15K04692, JP17H05252 in Scientific Research on Innovative Areas "Photosynergetics,"and CREST, JST.

[1] F. Helmchen and W. Denk, Nat. Methods **2**, 932 (2005).

[2] B. H. Cumpston *et. al*, Nature **398**, 51 (1999).

[3] W. S. Warren, H. Rabitz, and M. Dahleh, Science **259**, 1581 (1993).

[4] J. Gea-Banacloche, Phys. Rev. Lett. **62** 1603 (1989).

[5] J. Javanainen and P.L. Gould, Phys. Rev. A. **41** 5088 (1990).

[6] N. Ph. Georgiades, E. S. Polzik, K. Edamatsu, H. J. Kimble, and A. S. Parkins, Phys. Rev. Lett. **75** 3426 (1995).

[7] B. E. A. Saleh, B. M. Jost, H-B Fei, and M. C. Teich, Phys. Rev. Lett. **80**, 3483 (1998).

[8] O. Roslyak, C. A. Marx, and S. Mukamel, Phys. Rev. A **79**, 033832 (2009).

[9] M. G. Raymer, A. H. Marcus, J. R. Widom, and D. L. P. Vitullo, J. Phys. Chem. B **117**, 15559 (2013).

[10] F. Schlawin, K. E. Dorfman, and S. Mukamel, Phys. Rev. A **93**, 023807 (2016).

[11] K. E. Dorfman, F. Schlawin, and S. Makamel, Rev. Mod. Phys. **88**, 045008 (2016).

[12] F. Schlawin, J. Phys. B: At. Mol. Opt. Phys. **50**, 203001 (2017).

[13] R. de J. León-Montiel, J. Svozilík, L. J. Salazar-Serrano, and J. P. Torres, New J. Phys. **15**, 053023 (2013).

[14] M. B. Nasr, B. E. A. Saleh, A. V. Sergienko, and M. C. Teich, Phys. Rev. Lett. **91**, 083601(2003).

[15] T. Ono, R. Okamoto, and S. Takeuchi, Nat. Commun. **4**, 2426 (2013).

[16] H. Oka, J. Chem. Phys. **134**, 124313 (2011).

[17] F. Schlawin and A. Buchleitner, New. J. Phys. **19**, 013009 (2017).

[18] H. Oka, J. Phys. B: At. Mol. Opt. Phys. **48**, 115503 (2015).

[19] S. E. Harris, Phys. Rev. Lett. **98**, 063602 (2007).

[20] A. Tanaka, R. Okamoto, H.-H. Lim, S. Subashchandran, M, Okano, L. Zhang, L. Kang, J. Chen, P. Wu, T. Hirohata, S. Kurimura, and S. Takeuchi, Opt. Express **20**, 25228 (2012).

[21] H. Oka, Phys. Rev. A **97**, 033814 (2018).

[22] P. M. Morse, Phys. Rev. **34**, 57 (1929).

[23] T. Baumert, M. Grosser, R. Thalweiser, and G. Gerber, Phys. Rev. Lett. **67**, 3753 (1991).

[24] S. Magnier, Ph. Millié, O. Dulieu, and F. Masnou-Seeuws, J. Chem. Phys. **98**, 7113 (1993).

[25] H. Oka, Phys. Rev. A **81**, 053837 (2010).

[26] H. Oka, Phys. Rev. A **81**, 063819 (2010).

[27] V. Vedral, M. B. Plenio, M. A. Rippin, and P. L. Knight, Phys. Rev. Lett. **78**, 2275 (1997).

[28] W. K. Wootters, Phys. Rev. Lett. **80**, 2245 (1998).

[29] J. Flick, M. Ruggenthaler, H. Appel and A. Rubio, Proc. Natl. Acad. Sci. **114**, 3026 (2017).

[30] M. Kowalewski and S. Mukamel, Proc. Natl. Acad. Sci. **114** 3278 (2017).

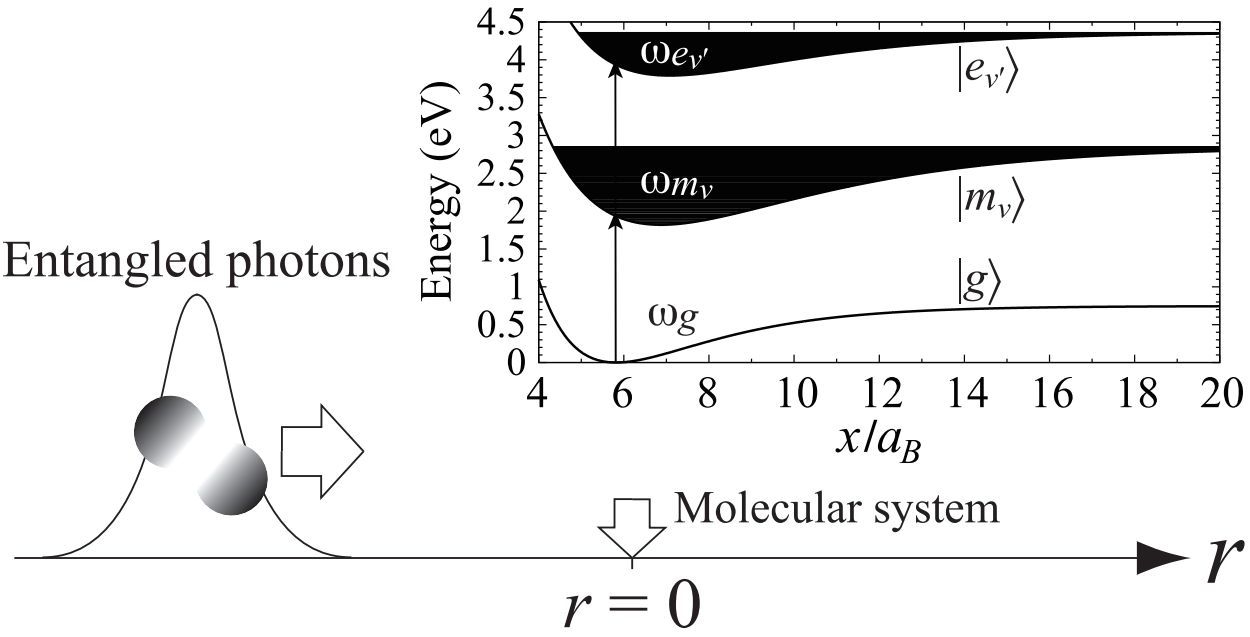

FIG. 1: Schematic of a one-dimensional photon field interacting with Morse oscillators. The eigenenergies ω_{m_v} and $\omega_{e_{v'}}$ of vibronic modes are calculated up to $v = 140$ and $v' = 89$, respectively.

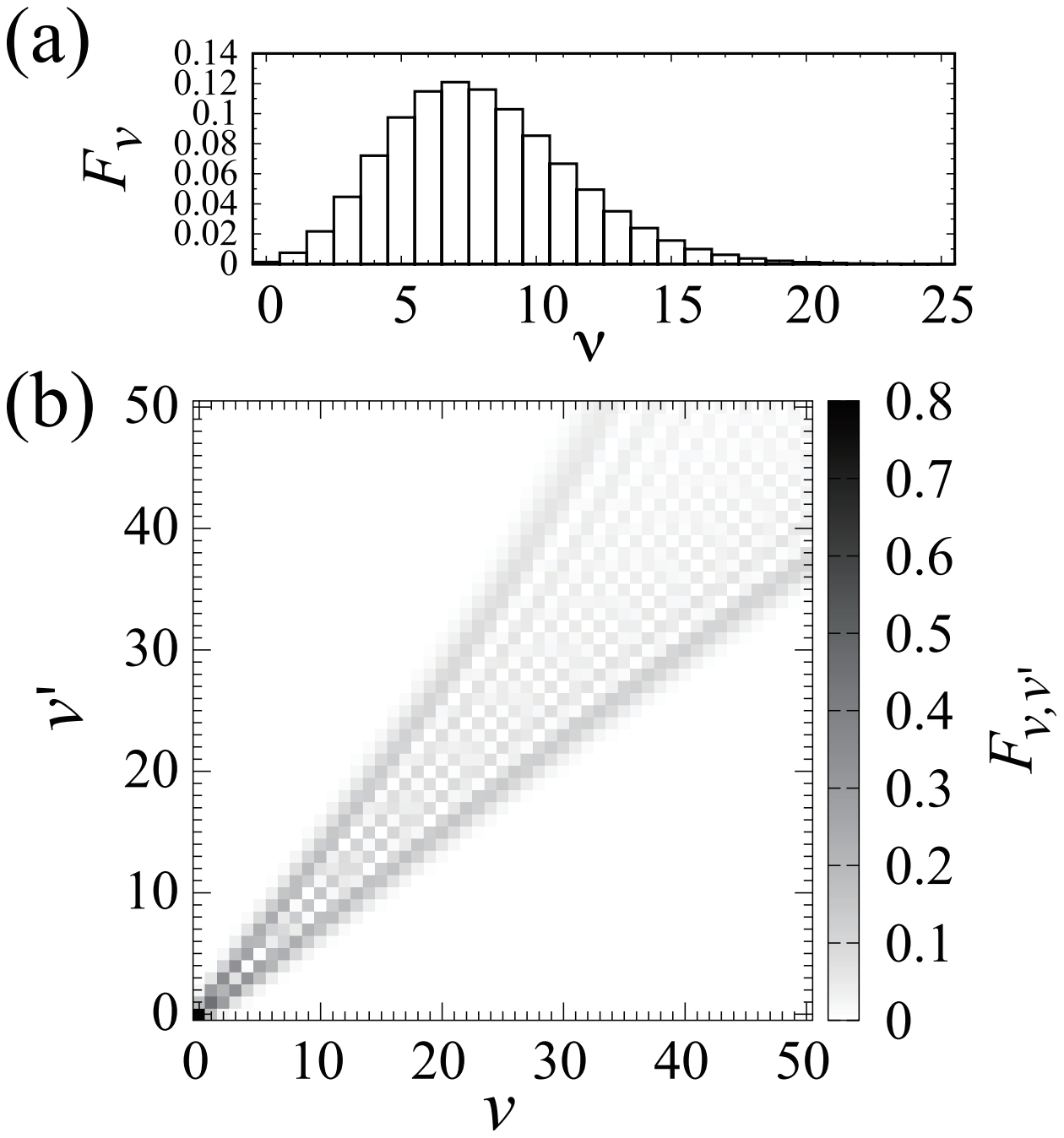

FIG. 2: (a) F_v as a function of v. (b) Contour plot of $F_{v,v'}$ as a function of v and v'.

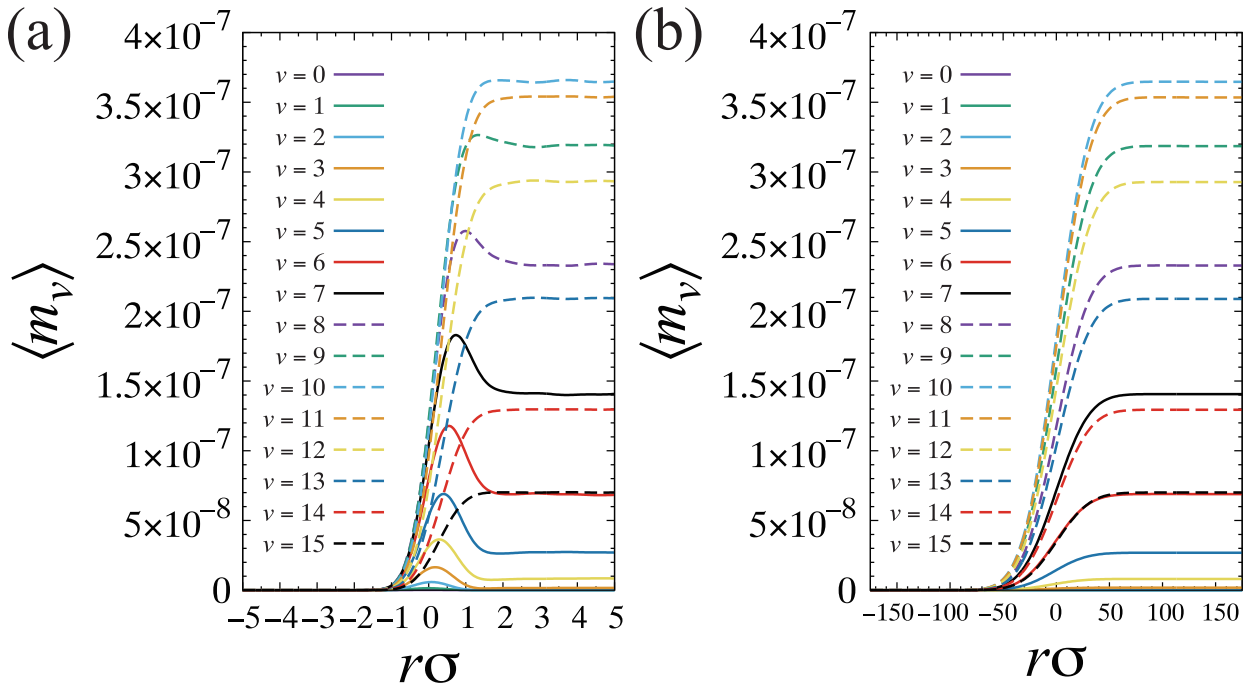

FIG. 3: The dynamics of $\langle m \rangle$ as a function of $r\sigma$: (a) uncorrelated photons and (b) entangled photons with $\sigma = 10$ THz.

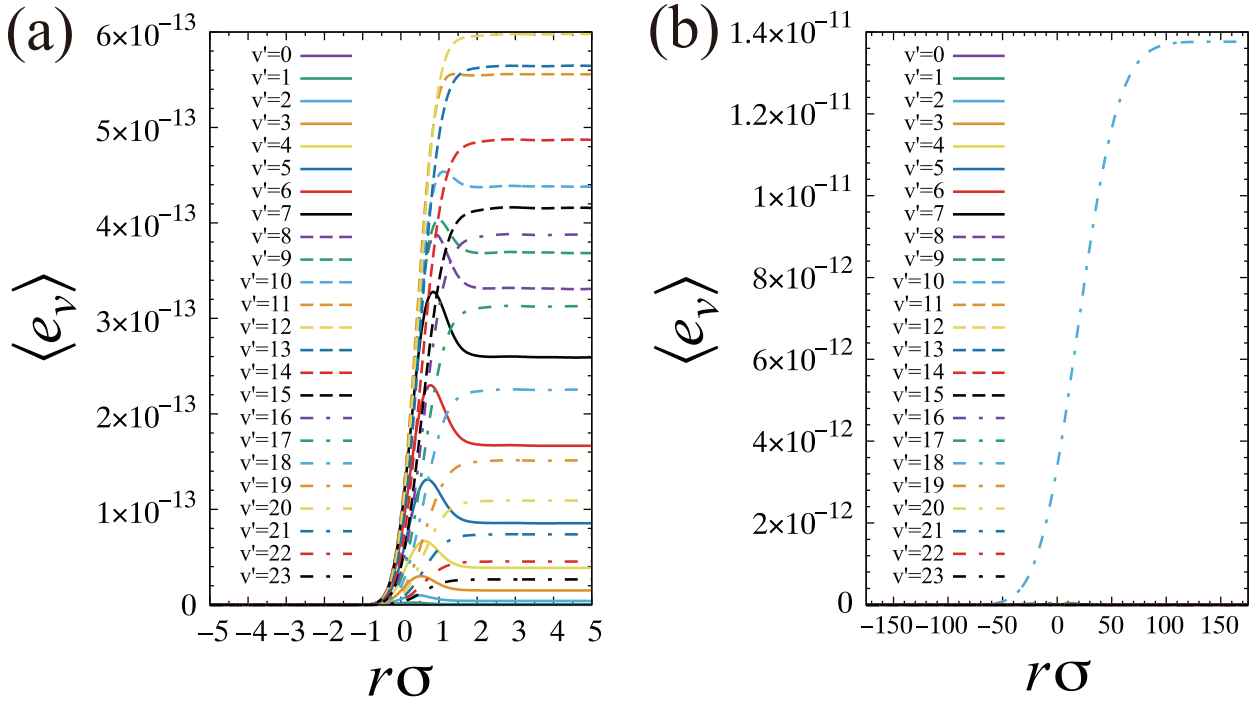

FIG. 4: The dynamics of $\langle e \rangle$ as a function of $r\sigma$: (a) uncorrelated photons and (b) entangled photons with $\sigma = 10$ THz.

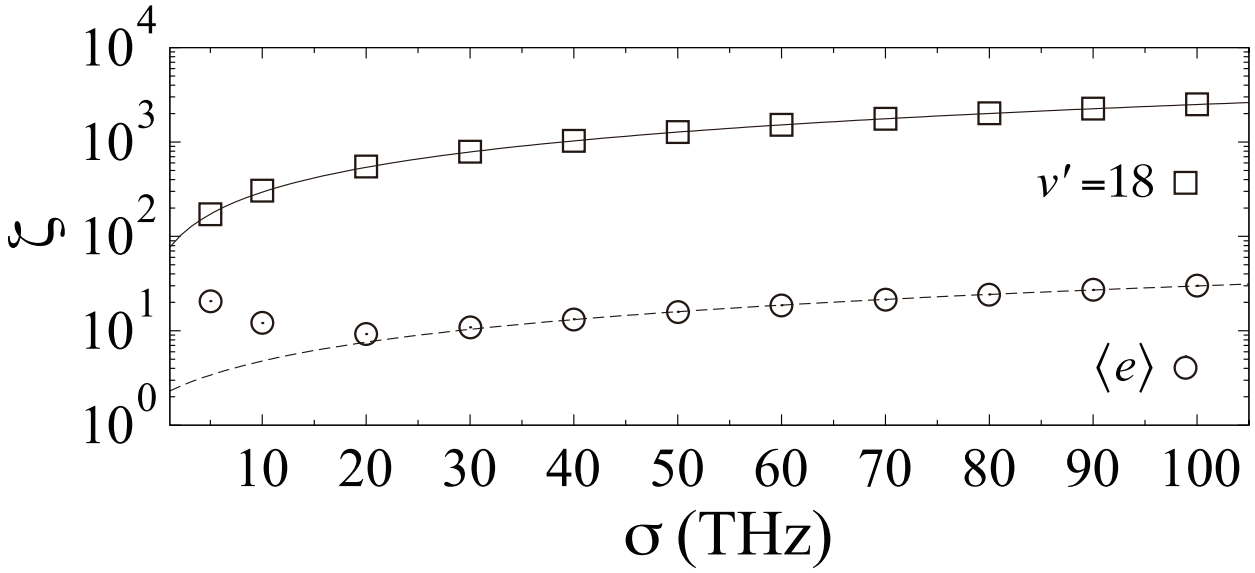

FIG. 5: ζ as a function of σ. The square $\square$ is for the vibrational mode of $v' = 18$ and the circle $\circ$ is for the total population of the excited state $\langle e \rangle$. The solid and dashed lines are to guide the reader's eye.

s

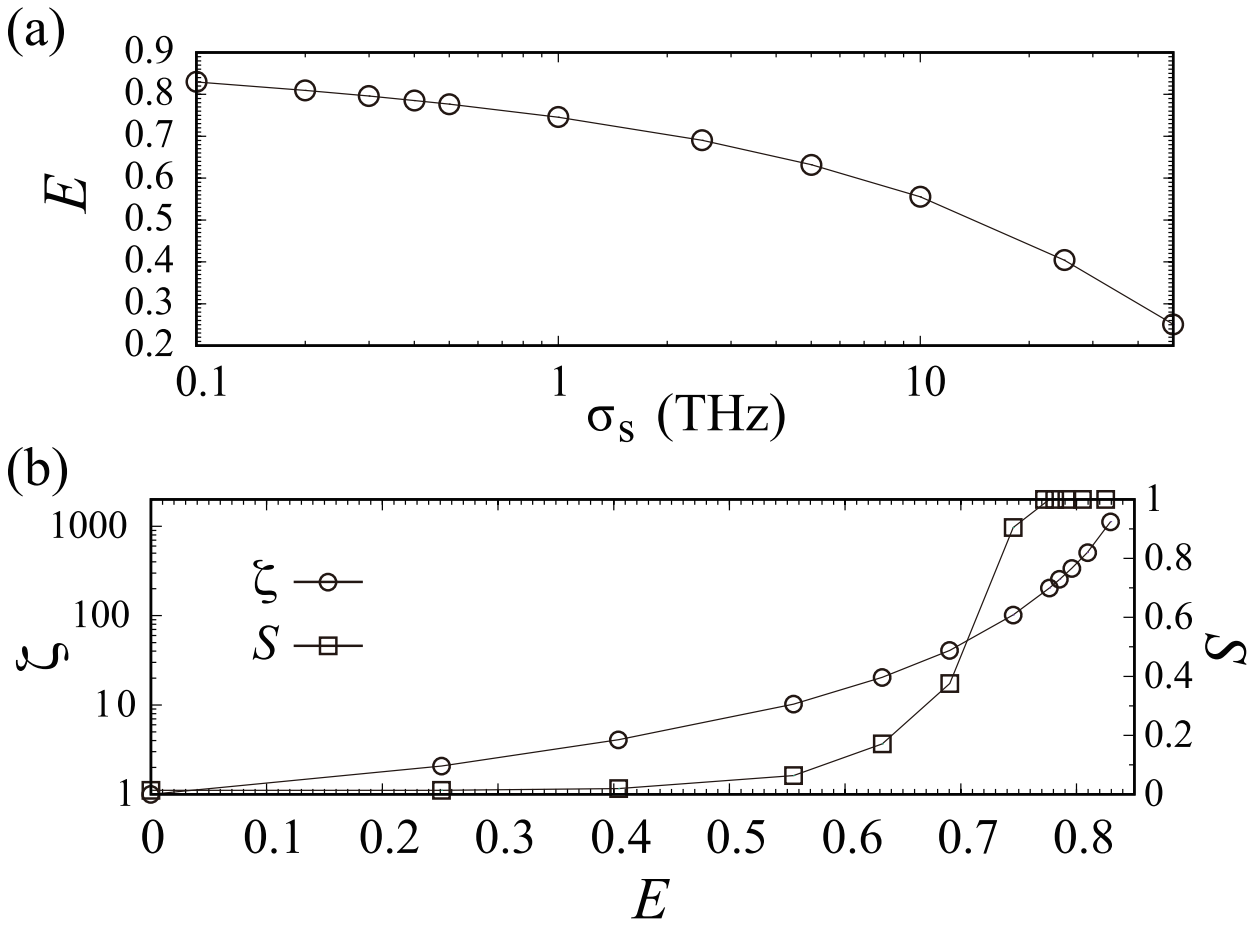

FIG. 6: (a) E as a function of σ_s. (b) ζ and S as a function of E. The solid lines are to guide the reader's eye.